APL Photonics

RESEARCH ARTICLE | DECEMBER 12 2023

# Programmable access to microresonator solitons with modulational sideband heating

Huamin Zheng ; Wei Sun ; Xingxing Ding ; Haoran Wen; Ruiyang Chen; Baoqi Shi ; Yi-Han Luo ; Jinbao Long; Chen Shen ; Shan Meng; Hairun Guo ; Junqiu Liu

Check for updates

*APL Photonics* 8, 126110 (2023)
https://doi.org/10.1063/5.0173243

View Online
Export Citation

31 July 2024 01:40:19

AMERICAN ELEMENTS
THE MATERIALS SCIENCE MANUFACTURER®
Now Invent.™
27 ANNIVERSARY
American Elements
Opens a World of Possibilities
...Now Invent!
www.americanelements.com

AIP Publishing

# Programmable access to microresonator solitons with modulational sideband heating

Cite as: APL Photon. 8, 126110 (2023); doi: 10.1063/5.0173243
Submitted: 21 August 2023 • Accepted: 13 November 2023 •
Published Online: 12 December 2023

View Online Export Citation CrossMark

Huamin Zheng,[1,2] Wei Sun,[2,a)] Xingxing Ding,[3] Haoran Wen,[2,4] Ruiyang Chen,[2,5] Baoqi Shi,[2,6] Yi-Han Luo,[2,5] Jinbao Long,[2] Chen Shen,[2] Shan Meng,[1] Hairun Guo,[3] and Junqiu Liu[2,7,b)]

## AFFILIATIONS

[1] College of Electronics and Information Engineering, Shenzhen University, Shenzhen 518000, China
[2] International Quantum Academy, Shenzhen 518048, China
[3] Key Laboratory of Specialty Fiber Optics and Optical Access Networks, Shanghai University, Shanghai 200444, China
[4] School of Science and Engineering, CUHK(SZ), Shenzhen 518100, China
[5] Shenzhen Institute for Quantum Science and Engineering, Southern University of Science and Technology, Shenzhen 518055, China
[6] Department of Optics and Optical Engineering, University of Science and Technology of China, Hefei 230026, China
[7] Hefei National Laboratory, University of Science and Technology of China, Hefei 230088, China

[a)] sunwei@iqasz.cn
[b)] **Author to whom correspondence should be addressed:** liujq@iqasz.cn

31 July 2024 01:40:19

## ABSTRACT

Dissipative Kerr solitons formed in high-$Q$ optical microresonators provide a route to miniaturized optical frequency combs that can revolutionize precision measurements, spectroscopy, sensing, and communication. In the past decade, a myriad of integrated material platforms have been extensively studied and developed to create photonic-chip-based soliton combs. However, the photo-thermal effect in integrated optical microresonators has been a major issue preventing simple and reliable soliton generation. Several sophisticated techniques to circumvent the photo-thermal effect have been developed. In addition, instead of the single-soliton state, emerging applications in microwave photonics and frequency metrology prefer multi-soliton states. Here, we demonstrate an approach to manage the photo-thermal effect and facilitate soliton generation. The approach is based on a single phase-modulated pump, where the generated blue-detuned sideband synergizes with the carrier and thermally stabilizes the microresonator. We apply this technique and demonstrate deterministic soliton generation of 19.97 GHz repetition rate in an integrated silicon nitride microresonator. Furthermore, we develop a program to automatically address to the target $N$-soliton state, in addition to the single-soliton state, with a near 100% success rate and as short as 10 s time consumption. Our method is valuable for soliton generation in essentially any platform, even with strong photo-thermal effects, and can promote wider applications of soliton frequency comb systems for microwave photonics, telecommunications, and frequency metrology.

*© 2023 Author(s). All article content, except where otherwise noted, is licensed under a Creative Commons Attribution (CC BY) license (http://creativecommons.org/licenses/by/4.0/).* https://doi.org/10.1063/5.0173243

## I. INTRODUCTION

Dissipative Kerr solitons formed in high-$Q$ optical microresonators[1,2] constitute miniaturized optical frequency combs with broad bandwidths and repetition rates in the microwave to millimeter-wave domain. Commonly referred to as "soliton microcombs," they have already been used in many system-level information and metrology applications, such as coherent telecommunication,[3–5] ultrafast ranging,[6,7] astronomical spectrometer calibration,[8,9] dual-comb spectroscopy,[10,11] low-noise microwave generation,[12,13] photonic neural networks,[14,15] datacenter circuit switches,[16] microwave photonics,[17,18] frequency synthesizers,[19] and optical atomic clocks.[20] Critical to the rapid progress of soliton microcomb technology is the development and continuous optimization of various photonic integrated platforms, including silica,[21,22] silicon nitride ($Si_3N_4$),[23,24] high-index doped silica (Hydex),[25,26] aluminum nitride (AlN),[27,28] lithium niobate ($LiNbO_3$),[29,30] tantala pentaoxide ($Ta_2O_5$),[31] silicon


© Author(s) 2023

carbide (SiC),[32,33] chalcogenide,[34] aluminum gallium arsenide (AlGaAs),[35,36] and gallium phosphide (GaP).[37] In addition, the introduction and successful implementation of hybrid and heterogeneous integration[38–44] further enable complex control schemes, extra nonlinearity, and efficient amplification for integrated soliton microcombs.

Despite these advances, one issue that currently prevents a wider deployment of soliton microcombs is how to deterministically access and control the soliton state. This issue is caused by the photo-thermal effect, arising from light absorption, and the thermal-optic effect in optical microresonators,[45,46] particularly those built on integrated platforms. When the continuous-wave (CW) pump's frequency is scanned through a microresonator resonance, from the blue-detuned side to the red-detuned side, a self-organized pulse waveform (i.e., a soliton state) is formed.[1] However, the photo-thermal effect leads to serious thermal instability that often annihilates the soliton state immediately. Therefore, sophisticated techniques to manage this effect have been developed, such as power kicking,[47,48] single-sideband suppressed-carrier frequency shifters,[49] dual-laser pumps,[50–54] pump modulation,[55–59] pulse pumping,[60] or laser self-cooling.[61,62] In addition, cryogenic operations can be helpful.[36] In addition, instead of the single-soliton state, efforts have also been made to employ multi-soliton states for reconfigurable photonic microwave filters[18] and the synthesis of terahertz frequencies.[63] For frequency metrology applications, the local comb line power enhancement in the multi-soliton state further facilitates the realization of self-referencing.[64]

Here, we demonstrate an approach to manage the photo-thermal effect, which enables automatic and deterministic access to a soliton state. This method, employing single-sideband heating, overcomes the photo-thermal effect in integrated microresonators. We apply this method to demonstrate that $N$-soliton states of 19.97 GHz repetition rate can be deterministically generated for any assigned value of $N \leq 5$.

## II. SOLITON STEP EXTENSION VIA SIDEBAND HEATING

The principle to excite a soliton state in a high-$Q$ optical microresonator with a single continuous-wave (CW) pump laser is shown in Fig. 1(a) top. As the pump laser scans through a resonance from its blue-detuned to the red-detuned side, the resonance is distorted from a Lorentzian to a triangular profile.[65] This change is due to the increasing intra-cavity power, which, via the photo-thermal effect, levitates the microresonator's temperature and extends its total optical length. Therefore, the "hot" resonance shifts following the direction of laser scanning. In this case, solitons can form on

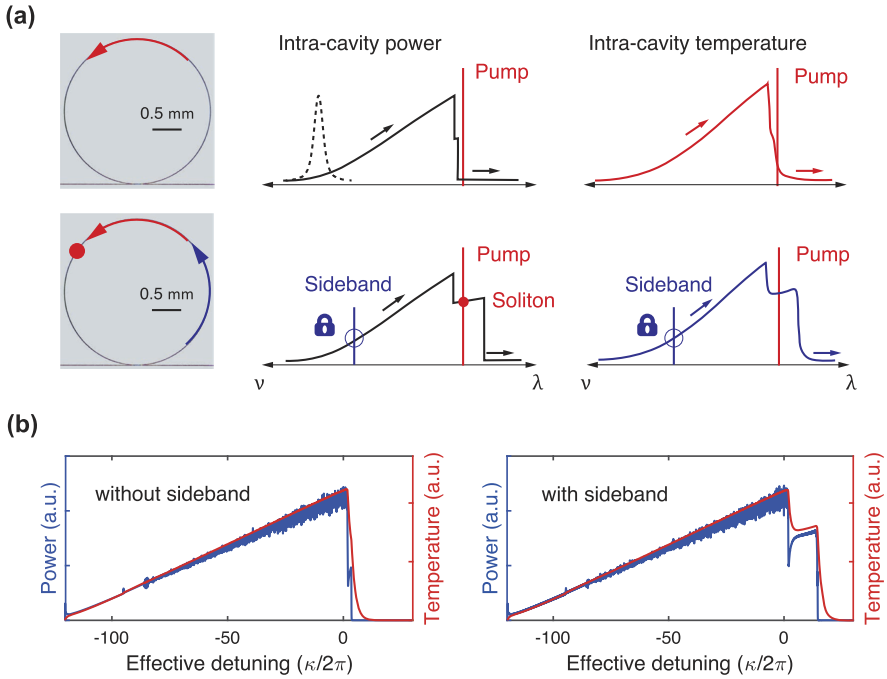


**FIG. 1.** Principle and numerical simulation of soliton generation in optical microresonators assisted with sideband heating. (a) Comparison of soliton step length without (top row) and with (bottom row) sideband heating. The left column shows the photos of the same $Si_3N_4$ microresonator of 19.97 GHz FSR. The red and blue arc arrows represent the CW carrier pump and the blue-detuned sideband. The middle column shows the intra-cavity power dynamics (solid black line) and the "cold" resonance (dashed black line). The right column shows the intra-cavity temperature dynamics. If the scanning pump (red line) stops on the soliton step, a soliton state is formed (red spot). Such a process can be facilitated by the blue-detuned sideband (blue line), which locks the "hot" resonance, avoids its shift, and extends the soliton step. (b) Numerical simulation of the intra-cavity power (blue) and temperature (red), without (left) and with (right) the blue-detuned sideband. The simulation reveals a soliton step extension due to the blue-detuned sideband.

31 July 2024 01:40:19


© Author(s) 2023

the red-detuned side of the effective resonance. A signature indicating soliton states is a series of step features ("soliton step") in the intra-cavity power,[66] as shown in Fig. 1(a). However, once a soliton state is reached, the intra-cavity power, as well as the microresonator temperature, drops suddenly. This leads to a sudden blue-shift of the resonance, which in turn increases the effective soliton-pump detuning. Therefore, this transition often compromises the soliton stability, causes extremely short or even negligible soliton steps, and often annihilates solitons immediately.

To circumvent such thermally induced instability, here we develop a blue-detuned sideband heating scheme to balance the sudden cooling of the microresonator during soliton formation. The principle is depicted in Fig. 1(a) at bottom. With proper frequency and power differences between the pump laser and its sideband, wherever the resonance moves, the sideband will drag the resonance back. For example, when the resonance experiences a sudden blue-shift during the transition from modulation instability to a soliton state, more optical power from the sideband enters the resonance, which levitates the microresonator's temperature to counteract the cooling. In such a way, the microresonator's intra-cavity power and temperature are locked, and the soliton step is extended, facilitating soliton formation.

A modified Lugiato–Lefever Equation (LLE) model to simulate soliton formation is considered as follows:

$$\frac{\partial}{\partial t}A(t,\varphi) = -\frac{\kappa}{2}A(t,\varphi) - i[\delta_\omega + g_\omega|A|^2 + \mathcal{D}_\omega + T]A(t,\varphi) + \sqrt{\kappa_{ex}}A_{in}, \tag{1}$$

where $A(t,\varphi)$ is the intra-cavity field amplitude, $\kappa = \kappa_0 + \kappa_{ex}$ is the total optical loss rate (with $\kappa_0$ being the intrinsic loss rate and $\kappa_{ex}$ being the external coupling rate with the input pump laser), $\delta_\omega$ is the soliton detuning, $g_\omega$ is the nonlinear coefficient, $\mathcal{D}_\omega$ is the microresonator dispersion, $T$ is the microresonator temperature, $A_{in} = \sqrt{P_{in}}(1 + \delta_m \exp(+i2\pi f_m t))$ is the input laser amplitude, $P_{in}$ is the input pump laser power, $P_{in}\delta_m^2$ is the input sideband power, and $f_m$ is the frequency difference between the pump laser and the sideband. The temperature of the cavity is proportional to its induced frequency shift $T$, which evolves following the equation:

$$\frac{\partial T}{\partial t} = \frac{K_T}{\tau_r}|A(t,\varphi)|^2 - \frac{T}{\tau_r}, \tag{2}$$

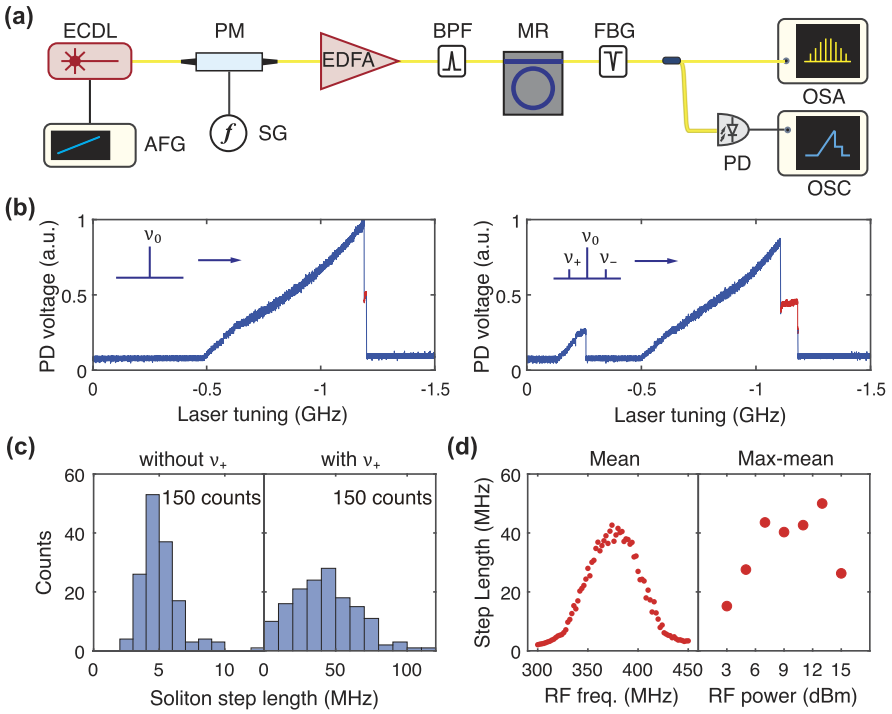


**FIG. 2.** Experimental demonstration of soliton step extension using sideband heating. (a) Experimental setup. ECDL: external-cavity diode laser. AFG: arbitrary function generator. PM: phase modulator. SG: signal generator. EDFA: erbium-doped fiber amplifier. BPF: bandpass filter. MR: $Si_3N_4$ microresonator. FBG: fiber Bragg grating. PD: photodiode. OSA: optical spectrum analyzer. OSC: oscilloscope. (b) Experimentally detected light generation from the microresonator, showing soliton step extension with the sideband. $\nu_0$: pump laser frequency. $\nu_+$: blue-detuned sideband frequency. $\nu_-$: red-detuned sideband frequency, which is idle in soliton generation. $\nu_\pm$ are generated by phase-modulating the pump laser with 396 MHz RF frequency and 11 dBm RF power on the phase modulator. The arrows indicate that the laser frequency is decreasing. The red-colored segments are soliton steps. In the right panel, with the sideband, the small triangular peak is due to $\nu_-$, the major triangular peak is due to $\nu_0$, and the soliton step is extended due to $\nu_+$. (c) Statistical analysis of 150 measured soliton step length values without (left) and with (right) the sideband $\nu_+$. The mean soliton step length is increased from 5.2 MHz (left) to 42.7 MHz (right). (d) Left: With 11 dBm RF power, the dependence of soliton step length on RF frequency. Right: The maximum value of step length for a given RF power with varying RF frequency. The best combination found in our experiment was 352 MHz RF frequency and 13 dBm RF power.

31 July 2024 01:40:19


© Author(s) 2023

where $K_T$ is the thermal-induced resonance shift coefficient and $\tau_r$ is the thermal relaxation time. With a proper set of parameters (see the supplementary material), the simulation shows prominent efficacy for thermal stabilization and soliton step extension, as shown in Fig. 1(b).

Experimentally, we create the sideband by phase-modulation of the carrier pump laser. The experimental setup is shown in Fig. 2(a). The pump laser is an external-cavity diode laser (ECDL, Toptica CTL 1550) with its frequency $\nu_0$ tuned by a piezo, which is actuated by an arbitrary function generator (AFG, Rigol DG4062). A phase modulator (PM, iXblue LPZ-LN-10) creates two sidebands ($\nu_-$ and $\nu_+$) from the carrier pump laser. The modulated laser is then power-amplified by an erbium-doped fiber amplifier (EDFA, KEOPSYS CEFA-C-PB-HP). A band-pass filter is applied to reject amplifier spontaneous emission (ASE) noise from the EDFA. After that, the laser power is coupled into an integrated silicon nitride ($Si_3N_4$) optical microresonator fabricated using a DUV subtractive process.[67] The $Si_3N_4$ microresonator features a 19.97 GHz free spectral range (FSR) and an intrinsic quality factor of $Q_0 \approx 1 \times 10^7$, characterized using a vector spectrum analyzer[68] (see the supplementary material). After the $Si_3N_4$ microresonator, the pump laser is blocked by two fiber Bragg gratings (FBG), providing 30 dB total attenuation. Finally, the output optical spectrum is monitored by an optical spectrum analyzer (OSA, Yokogawa AQ6370D). The optical power is detected by a photodiode (PD, Thorlabs PDA10CS2) and monitored by an oscilloscope (OSC, Rigol DHO4404).

The wavelength and power of the pump laser without phase modulation are 1555.7 nm and 730 mW, respectively. The pump laser's frequency scans through resonance from the effectively blue-detuned to the red-detuned side ("forward tuning"[1]), with the direction marked by arrows in Fig. 2(b). The light detected by the PD and recorded by the OSC corresponds to the generated light from Kerr parametric oscillation in the microresonator. The soliton step is marked with a red color within the total 1.5 GHz frequency range. Due to the photo-thermal effect in $Si_3N_4$, the soliton step is so short that it is barely seen, making it challenging to access a soliton state. However, when phase-modulating the pump laser with a modulation frequency of $f_m = 374$ MHz and RF power applied to the PM of 11 dBm, a pair of sidebands $\nu_\pm = \nu_0 \pm f_m$ are created. The carrier pump laser's power is 8.3 times higher than that of one sideband. Only the blue sideband $\nu_+$ is used to counteract the thermal effect,[56,57] while the red sideband $\nu_-$ is idle. Prominent soliton step extension is observed with the phase modulation, as shown in Fig. 2(b). We repeatedly scan the laser through the

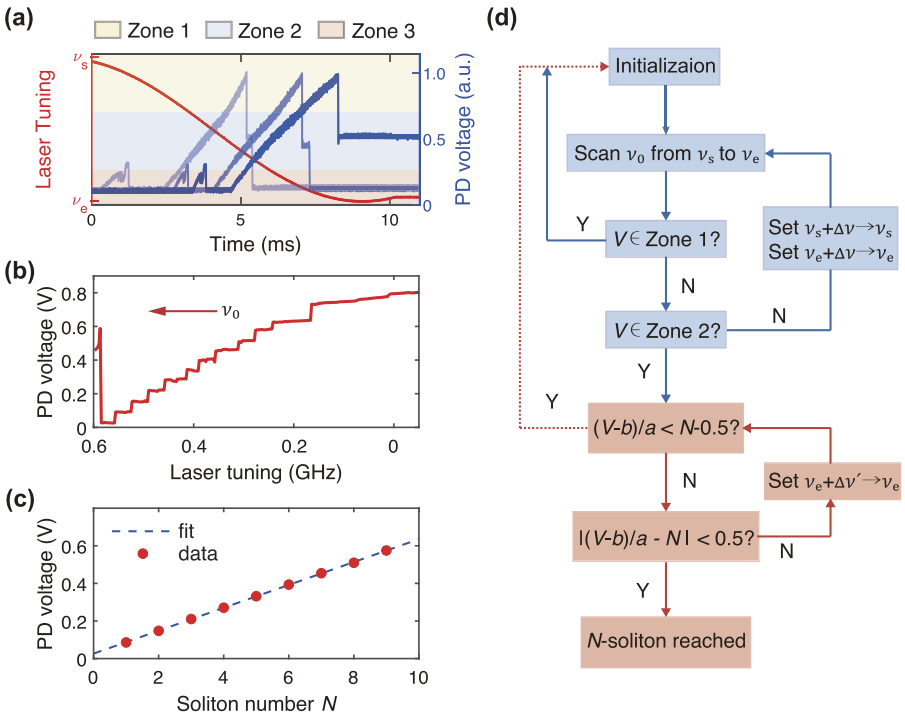


**FIG. 3.** Criteria and program for automatic *N*-soliton state addressing. (a) Generated light power dynamics labeled with different zones. The red curve shows that the laser frequency $\nu_0$ is decreasing from $\nu_s$ to $\nu_e$. The blue curves with different tones show the normalized power traces detected by the PD and recorded by the OSC. The traces together show the process of accessing a soliton state by translating $(\nu_s, \nu_e)$ with step $\Delta\nu$, as shown in panel (d). Zones 1/2/3 are marked and only zone 2 supports soliton formation. (b) Using the backward-tuning process, the power trace measured by the PD shows a stair feature, which contains many steps corresponding to soliton states with a different soliton number *N*. The arrow indicates that the laser frequency is increasing. (c) The backward-tuning soliton generation process is repeated 20 times, and the average PD voltage $\overline{V}$ for each step is fitted with the soliton number *N*, resulting in a linear relation of $\overline{V} = a \times N + b$ ($a = 0.0609, b = 0.0265$). (d) The logic codes and algorithm flowchart for computer-controlled automatic *N*-soliton state generation. The blue-colored block is for soliton generation, and the red-colored block is for *N*-soliton state addressing. The solid lines with arrows represent successful addressing, and the dashed line with arrows represents failed addressing.

31 July 2024 01:40:19


© Author(s) 2023

resonance 150 times and statistically analyze the soliton step length, as shown in Fig. 2(c). The statistical mean values are 5.2 and 42.7 MHz, respectively, corresponding to eight-times extension due to sideband heating. It is worth noting that the on-chip power of the blue sideband is 37 mW, which is sufficient to induce a prominent photo-thermal effect but insufficient to trigger Kerr parametric oscillation. In addition, we have not observed the generation of sub-comb lines due to the cross-phase modulation between the blue sideband and the soliton combines (see the supplementary material for detail).

We further investigate the optimal value of $f_m$ for maximum soliton step extension, as shown in Fig. 2(d) left. The optimal value under 11 dBm RF power is $f_m$ = 374 MHz. The effect of RF power on soliton step length is also investigated, as shown in Fig. 2(d) right.

## III. SOLITON NUMBER-STATE ADDRESSING

Next, we realize the deterministic generation of an $N$-soliton state using the sideband heating method. Figure 3(a) shows the dynamic PD voltage, i.e., the dynamically generated light power, where the soliton step sits in zone 2. The supplementary material shows that zone 2 covers the full range of detected voltages for all possible soliton steps in 50 time measurements. Zone 1 indicates that the laser frequency is effectively blue-detuned, and zone 3 indicates far red-detuned, neither of which allows soliton existence.

To distinguish the soliton number, we use the backward tuning scheme by increasing the laser frequency.[66] The soliton power trace probed by the PD is converted to a voltage trace that shows a clear stair feature in Fig. 3(b). Each step in the stair corresponds to a soliton state with a different $N$. We measure the mean voltage $\overline{V}$

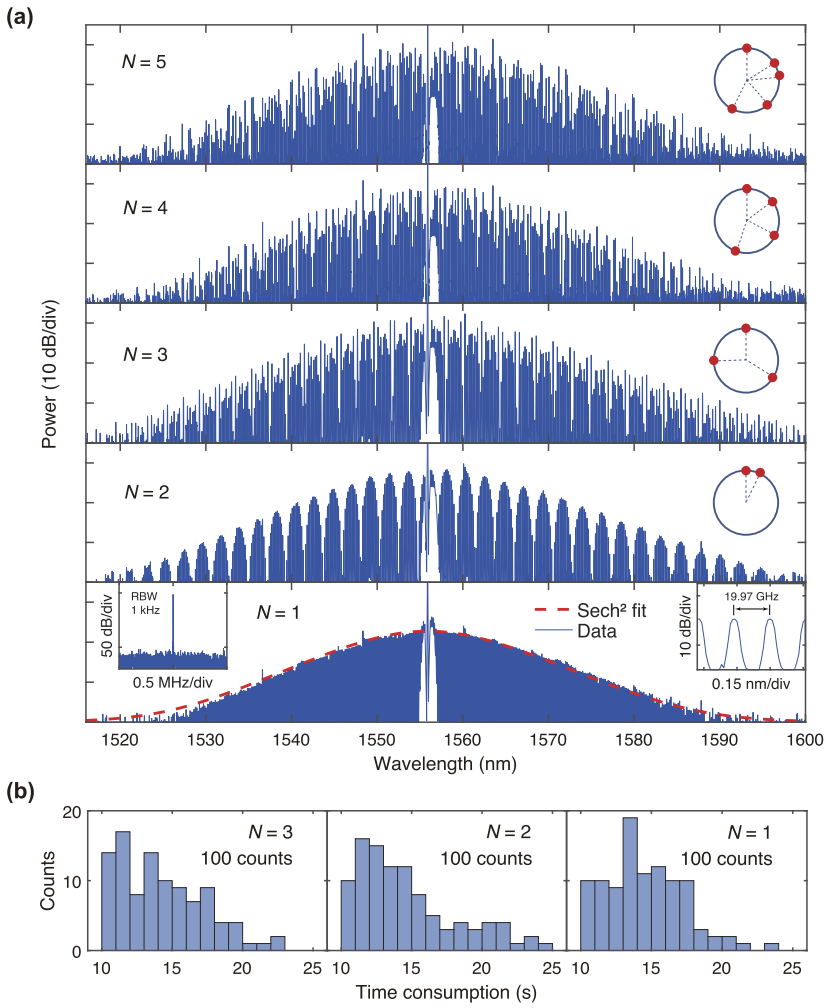


**FIG. 4.** Single- and multi-soliton spectra and the time consumption to reach these states. (a) Optical spectra for $N$ = 5, 4, 3, 2, 1-soliton states of 19.97 GHz mode spacing. Insets show the relative soliton positions of the $N$-soliton state in the microresonator. The soliton numbers $N$ are retrieved by the inverse Fourier transform on the spectrum. The single-soliton spectrum is fitted with a sech$^2$ function (dashed red line). In the diagram of the single-soliton optical spectrum, the left inset shows the RF power spectrum of the soliton repetition rate, and the right inset highlights the comb line spacing. (b) Statistics of time consumption for $N$ = 3, 2, 1-soliton state addressing with 100 repeated processes, among which 93/99/100 processes come into successful state addressing.

31 July 2024 01:40:19


© Author(s) 2023

values of each step and classify them into a different soliton number $N$. Figure 3(c) shows that, after repeating 20 times, a linear relation between the voltage and soliton number is found, i.e., $\overline{V} = a \times N + b$, with $a = 0.0609$ and $b = 0.0265$.

Previously, program-controlled single-soliton generation was realized with two lasers and integrated microresonators with repetition rates above 49 GHz[26,53,54] that are difficult to detect with normal fast photodetectors. Here, using only one laser and with calibrated zones and $(a, b)$ parameters, we demonstrate a program for deterministic generation of target $N$-soliton state in our $Si_3N_4$ microresonator with FSR down to 19.97 GHz, in addition to the single-soliton state. The program logic is shown in Fig. 3(d), which consists of two blocks. The first block (blue) is to land on a soliton step, and the second block (red) is to produce the target $N$-soliton state. Initially, the laser frequency scans from $\nu_s$ to $\nu_e$ ($\nu_s > \nu_e$) close to the resonance, such that the final PD voltage lands in zone 3, as shown by the lightest blue trace in Fig. 3(a). The scanning window is then translated by $\Delta\nu$, i.e., the laser is re-scanned from $\nu_s + \Delta\nu$ to $\nu_e + \Delta\nu$. After that, if the PD voltage lands in zone 1, meaning that the laser frequency is blue-detuned and the soliton state is missed, then the system is re-initiated. If the PD voltage still lands in zone 3, the laser frequency scanning window is further translated by $\Delta\nu$. The process continues until the PD voltage lands in zone 2, signaling that a soliton state is reached, as the darkest blue trace shows in Fig. 3(a).

When a soliton state is reached, the program's second block starts. Using $(a, b)$ parameters and the PD voltage, the current soliton number is estimated by $(V - b)/a$. For a target soliton number $N$, if $(V - b)/a < N - 0.5$, the target $N$-soliton generation fails and the system is re-initiated. If $(V - b)/a > N + 0.5$, the laser frequency is increased with step $\Delta\nu'$ until $(V - b)/a \in [N - 0.5, N + 0.5]$, where the $N$-soliton state is successfully produced. Parameters $(\Delta\nu, \Delta\nu')$ are self-adaptive and modified to accelerate the sequence (see the supplementary material).

We repeatedly apply the program for automatic $N$-soliton generation 100 times. The soliton number $N$ can be retrieved by inverse Fourier transform on the soliton's optical spectrum on OSA, as shown in Fig. 4(a). We verify the soliton number of every addressed $N = 5, 4, 3, 2, 1$-soliton state. The RF power spectrum of the single-soliton repetition rate is shown in the left inset of Fig. 4(a), where the coherence of comb lines is revealed from the pure single RF signal with a signal-to-noise ratio exceeding 50 dB at 1 kHz resolution bandwidth. The statistic charts of time consumption for the $N = 3, 2, 1$-soliton state addressing are shown in Fig. 4(b). The success rates are 93%, 99%, and 100% for $N = 3, 2, 1$-soliton production, respectively. In the backward tuning process, the soliton number can be reduced by two or more, especially when the soliton number is large (which is true for microresonators with a small FSR), so that the success rate of multiple solitons is not 100%. Table I summarizes the data of up to 5-soliton production. The maximum $N = 9$ soliton state can be addressed, while the $N > 9$-soliton state is challenging to distinguish due to the large power variation. The existence of the $N$-soliton state is monitored by sampling the PD voltage $V$ at 10 Hz rate.

**TABLE I.** Statistics of success rate and time consumption to produce $N$-soliton states.

| Soliton number $N$ | Success rate (%) | Probability <15 s (%) | Probability <20 s (%) | Mean time (s) | Shortest time (s) |
|---|---|---|---|---|---|
| 1 | 100 | 59 | 96 | 14.6 | 10.6 |
| 2 | 99 | 65 | 88 | 14.7 | 10.3 |
| 3 | 93 | 63 | 96 | 14.3 | 10.1 |
| 4 | 96 | 45 | 72 | 17.5 | 9.9 |
| 5 | 95 | 47 | 80 | 16.7 | 2.8 |

## IV. CONCLUSION

In conclusion, we have demonstrated a novel experimental approach to manage the photo-thermal effect commonly encountered in the generation of dissipative Kerr solitons in optical microresonators. The approach is based on phase-modulation of the CW pump, where the generated blue sideband synergizes with the carrier pump and thermally stabilizes the microresonator. The sideband provides immediate heating when the intra-cavity power transits to a soliton state and the microresonator experiences a sudden cooling. Using a 19.97-GHz-FSR $Si_3N_4$ microresonator, we successfully demonstrated soliton step extension by more than eight times with the sideband heating. Furthermore, we have developed a program to automatically, deterministically, and quickly address to target $N$-soliton state, including the single-soliton state. We show a near 100% success rate and as short as 10 s time consumption for $N$-soliton state addressing.

While demonstrated on $Si_3N_4$, our method is also useful for soliton generation in other platforms suffering from stronger photo-thermal effects. Experimentally, one can choose a proper power level of the blue sideband (which is sufficient to induce a photo-thermal effect but insufficient to trigger Kerr parametric oscillation) and then manually search for the ideal modulation frequency on the CW pump to generate the blue sideband. With few iterations, the ideal combination of modulational power and frequency is acquired. The program-controlled automatic addressing of the $N$-soliton state can be critical for several applications in microwave photonics and frequency comb metrology. Together, our method facilitates a wider range of applications of soliton microcomb systems outside of laboratory environments.

## SUPPLEMENTARY MATERIAL

See the supplementary material for details on the simulation, chip characterization, determination of zone 2, sequence acceleration for $N$-soliton state addressing, and nonlinear effect of the blue sideband.

## ACKNOWLEDGMENTS

We thank Yuan Chen, Sanli Huang, and Zhongkai Wang for their assistance in the experiment, Suwan Sun for his assistance in the simulation, and Jijun He for the fruitful discussion. J. Liu acknowledges the support from the National Natural Science Foundation of China (Grant No. 12261131503), the Shenzhen-Hong Kong Cooperation Zone for Technology and Innovation (Grant No. HZQB-KCZYB2020050), and the Guangdong Provincial

31 July 2024 01:40:19


© Author(s) 2023

Key Laboratory (Grant No. 2019B121203002). Y.-H.L. acknowledges the support from the China Postdoctoral Science Foundation (Grant No. 2022M721482). Hairun Guo acknowledges the support from the National Natural Science Foundation of China (Grant No. 11974234). Silicon nitride chips were fabricated by Qaleido Photonics.

## AUTHOR DECLARATIONS

### Conflict of Interest

W. S., J. Long and J. Liu filed a patent application related to this work. Others declare no conflicts of interest.

### Author Contributions

**Huamin Zheng**: Data curation (equal); Formal analysis (equal); Investigation (equal); Methodology (equal); Software (equal); Validation (equal); Visualization (supporting); Writing – review & editing (equal). **Wei Sun**: Conceptualization (equal); Data curation (equal); Formal analysis (equal); Investigation (equal); Methodology (equal); Software (equal); Validation (equal); Visualization (lead); Writing – original draft (equal); Writing – review & editing (equal). **Xingxing Ding**: Software (equal); Visualization (supporting); Writing – review & editing (equal). **Haoran Wen**: Data curation (equal); Formal analysis (equal); Investigation (supporting); Visualization (supporting); Writing – review & editing (equal). **Ruiyang Chen**: Software (supporting); Visualization (supporting); Writing – review & editing (equal). **Baoqi Shi**: Investigation (supporting); Visualization (supporting); Writing – review & editing (equal). **Yi-Han Luo**: Funding acquisition (supporting); Software (supporting); Visualization (supporting); Writing – review & editing (equal). **Jinbao Long**: Investigation (equal). **Chen Shen**: Resources (equal). **Shan Meng**: Investigation (supporting). **Hairun Guo**: Funding acquisition (supporting); Software (equal); Writing – review & editing (equal). **Junqiu Liu**: Conceptualization (equal); Formal analysis (equal); Funding acquisition (lead); Methodology (equal); Project administration (lead); Resources (equal); Supervision (lead); Validation (equal); Visualization (supporting); Writing – original draft (equal); Writing – review & editing (equal).

## DATA AVAILABILITY

The code and data that support the findings of this study are openly available in Zenodo (https://doi.org/10.5281/zenodo.10158216).

## REFERENCES

[1]T. Herr, V. Brasch, J. D. Jost, C. Y. Wang, N. M. Kondratiev, M. L. Gorodetsky, and T. J. Kippenberg, "Temporal solitons in optical microresonators," Nat. Photonics **8**, 145 (2013).

[2]T. J. Kippenberg, A. L. Gaeta, M. Lipson, and M. L. Gorodetsky, "Dissipative Kerr solitons in optical microresonators," Science **361**, eaan8083 (2018).

[3]P. Marin-Palomo, J. N. Kemal, M. Karpov, A. Kordts, J. Pfeifle, M. H. P. Pfeiffer, P. Trocha, S. Wolf, V. Brasch, M. H. Anderson, R. Rosenberger, K. Vijayan, W. Freude, T. J. Kippenberg, and C. Koos, "Microresonator-based solitons for massively parallel coherent optical communications," Nature **546**, 274 (2017).

[4]B. Corcoran, M. Tan, X. Xu, A. Boes, J. Wu, T. G. Nguyen, S. T. Chu, B. E. Little, R. Morandotti, A. Mitchell, and D. J. Moss, "Ultra-dense optical data transmission over standard fibre with a single chip source," Nat. Commun. **11**, 2568 (2020).

[5]M. Mazur, M.-G. Suh, A. Fülöp, J. Schröder, V. Torres-Company, M. Karlsson, K. Vahala, and P. Andrekson, "High spectral efficiency coherent superchannel transmission with soliton microcombs," J. Lightwave Technol. **39**, 4367–4373 (2021).

[6]P. Trocha, M. Karpov, D. Ganin, M. H. P. Pfeiffer, A. Kordts, S. Wolf, J. Krockenberger, P. Marin-Palomo, C. Weimann, S. Randel, W. Freude, T. J. Kippenberg, and C. Koos, "Ultrafast optical ranging using microresonator soliton frequency combs," Science **359**, 887–891 (2018).

[7]M.-G. Suh and K. J. Vahala, "Soliton microcomb range measurement," Science **359**, 884–887 (2018).

[8]E. Obrzud, M. Rainer, A. Harutyunyan, M. H. Anderson, J. Liu, M. Geiselmann, B. Chazelas, S. Kundermann, S. Lecomte, M. Cecconi, A. Ghedina, E. Molinari, F. Pepe, F. Wildi, F. Bouchy, T. J. Kippenberg, and T. Herr, "A microphotonic astrocomb," Nat. Photonics **13**, 31–35 (2019).

[9]M.-G. Suh, X. Yi, Y.-H. Lai, S. Leifer, I. S. Grudinin, G. Vasisht, E. C. Martin, M. P. Fitzgerald, G. Doppmann, J. Wang, D. Mawet, S. B. Papp, S. A. Diddams, C. Beichman, and K. Vahala, "Searching for exoplanets using a microresonator astrocomb," Nat. Photonics **13**, 25–30 (2019).

[10]A. Dutt, C. Joshi, X. Ji, J. Cardenas, Y. Okawachi, K. Luke, A. L. Gaeta, and M. Lipson, "On-chip dual-comb source for spectroscopy," Sci. Adv. **4**, e1701858 (2018).

[11]Q.-F. Yang, B. Shen, H. Wang, M. Tran, Z. Zhang, K. Y. Yang, L. Wu, C. Bao, J. Bowers, A. Yariv, and K. Vahala, "Vernier spectrometer using counterpropagating soliton microcombs," Science **363**, 965–968 (2019).

[12]W. Liang, D. Eliyahu, V. S. Ilchenko, A. A. Savchenkov, A. B. Matsko, D. Seidel, and L. Maleki, "High spectral purity Kerr frequency comb radio frequency photonic oscillator," Nat. Commun. **6**, 7957 (2015).

[13]J. Liu, E. Lucas, A. S. Raja, J. He, J. Riemensberger, R. N. Wang, M. Karpov, H. Guo, R. Bouchand, and T. J. Kippenberg, "Photonic microwave generation in the X- and K-band using integrated soliton microcombs," Nat. Photonics **14**, 486–491 (2020).

[14]J. Feldmann, N. Youngblood, M. Karpov, H. Gehring, X. Li, M. Stappers, M. Le Gallo, X. Fu, A. Lukashchuk, A. S. Raja, J. Liu, C. D. Wright, A. Sebastian, T. J. Kippenberg, W. H. P. Pernice, and H. Bhaskaran, "Parallel convolutional processing using an integrated photonic tensor core," Nature **589**, 52–58 (2021).

[15]X. Xu, M. Tan, B. Corcoran, J. Wu, A. Boes, T. G. Nguyen, S. T. Chu, B. E. Little, D. G. Hicks, R. Morandotti, A. Mitchell, and D. J. Moss, "11 TOPS photonic convolutional accelerator for optical neural networks," Nature **589**, 44–51 (2021).

[16]A. S. Raja, S. Lange, M. Karpov, K. Shi, X. Fu, R. Behrendt, D. Cletheroe, A. Lukashchuk, I. Haller, F. Karinou, B. Thomsen, K. Jozwik, J. Liu, P. Costa, T. J. Kippenberg, and H. Ballani, "Ultrafast optical circuit switching for data centers using integrated soliton microcombs," Nat. Commun. **12**, 5867 (2021).

[17]J. Wu, X. Xu, T. G. Nguyen, S. T. Chu, B. E. Little, R. Morandotti, A. Mitchell, and D. J. Moss, "RF photonics: An optical microcombs' perspective," IEEE J. Sel. Top. Quantum Electron. **24**, 6101020 (2018).

[18]J. Hu, J. He, J. Liu, A. S. Raja, M. Karpov, A. Lukashchuk, T. J. Kippenberg, and C.-S. Brès, "Reconfigurable radiofrequency filters based on versatile soliton microcombs," Nat. Commun. **11**, 4377 (2020).

[19]D. T. Spencer, T. Drake, T. C. Briles, J. Stone, L. C. Sinclair, C. Fredrick, Q. Li, D. Westly, B. R. Ilic, A. Bluestone, N. Volet, T. Komljenovic, L. Chang, S. H. Lee, D. Y. Oh, M.-G. Suh, K. Y. Yang, M. H. P. Pfeiffer, T. J. Kippenberg, E. Norberg, L. Theogarajan, K. Vahala, N. R. Newbury, K. Srinivasan, J. E. Bowers, S. A. Diddams, and S. B. Papp, "An optical-frequency synthesizer using integrated photonics," Nature **557**, 81–85 (2018).

[20]Z. L. Newman, V. Maurice, T. Drake, J. R. Stone, T. C. Briles, D. T. Spencer, C. Fredrick, Q. Li, D. Westly, B. R. Ilic, B. Shen, M.-G. Suh, K. Y. Yang, C. Johnson, D. M. S. Johnson, L. Hollberg, K. J. Vahala, K. Srinivasan, S. A. Diddams, J. Kitching, S. B. Papp, and M. T. Hummon, "Architecture for the photonic integration of an optical atomic clock," Optica **6**, 680–685 (2019).

31 July 2024 01:40:19


© Author(s) 2023

[21]X. Yi, Q.-F. Yang, K. Y. Yang, M.-G. Suh, and K. Vahala, "Soliton frequency comb at microwave rates in a high-*Q* silica microresonator," Optica **2**, 1078–1085 (2015).
[22]K. Y. Yang, D. Y. Oh, S. H. Lee, Q.-F. Yang, X. Yi, B. Shen, H. Wang, and K. Vahala, "Bridging ultrahigh-*Q* devices and photonic circuits," Nat. Photonics **12**, 297–302 (2018).
[23]V. Brasch, M. Geiselmann, T. Herr, G. Lihachev, M. H. P. Pfeiffer, M. L. Gorodetsky, and T. J. Kippenberg, "Photonic chip-based optical frequency comb using soliton Cherenkov radiation," Science **351**, 357–360 (2016).
[24]C. Joshi, J. K. Jang, K. Luke, X. Ji, S. A. Miller, A. Klenner, Y. Okawachi, M. Lipson, and A. L. Gaeta, "Thermally controlled comb generation and soliton modelocking in microresonators," Opt. Lett. **41**, 2565–2568 (2016).
[25]H. Bao, A. Cooper, M. Rowley, L. Di Lauro, J. S. Totero Gongora, S. T. Chu, B. E. Little, G.-L. Oppo, R. Morandotti, D. J. Moss, B. Wetzel, M. Peccianti, and A. Pasquazi, "Laser cavity-soliton microcombs," Nat. Photonics **13**, 384–389 (2019).
[26]X. Wang, P. Xie, W. Wang, Y. Wang, Z. Lu, L. Wang, S. T. Chu, B. E. Little, W. Zhao, and W. Zhang, "Program-controlled single soliton microcomb source," Photonics Res. **9**, 66–72 (2021).
[27]X. Liu, Z. Gong, A. W. Bruch, J. B. Surya, J. Lu, and H. X. Tang, "Aluminum nitride nanophotonics for beyond-octave soliton microcomb generation and self-referencing," Nat. Commun. **12**, 5428 (2021).
[28]H. Weng, J. Liu, A. A. Afridi, J. Li, J. Dai, X. Ma, Y. Zhang, Q. Lu, J. F. Donegan, and W. Guo, "Directly accessing octave-spanning dissipative Kerr soliton frequency combs in an AlN microresonator," Photonics Res. **9**, 1351–1357 (2021).
[29]Y. He, Q.-F. Yang, J. Ling, R. Luo, H. Liang, M. Li, B. Shen, H. Wang, K. Vahala, and Q. Lin, "Self-starting bi-chromatic $LiNbO_3$ soliton microcomb," Optica **6**, 1138–1144 (2019).
[30]Z. Gong, X. Liu, Y. Xu, and H. X. Tang, "Near-octave lithium niobate soliton microcomb," Optica **7**, 1275–1278 (2020).
[31]H. Jung, S.-P. Yu, D. R. Carlson, T. E. Drake, T. C. Briles, and S. B. Papp, "Tantala Kerr nonlinear integrated photonics," Optica **8**, 811–817 (2021).
[32]M. A. Guidry, D. M. Lukin, K. Y. Yang, R. Trivedi, and J. Vučković, "Quantum optics of soliton microcombs," Nat. Photonics **16**, 52–58 (2022).
[33]C. Wang, J. Li, A. Yi, Z. Fang, L. Zhou, Z. Wang, R. Niu, Y. Chen, J. Zhang, Y. Cheng, J. Liu, C.-H. Dong, and X. Ou, "Soliton formation and spectral translation into visible on CMOS-compatible 4H-silicon-carbide-on-insulator platform," Light: Sci. Appl. **11**, 341 (2022).
[34]D. Xia, Z. Yang, P. Zeng, B. Zhang, J. Wu, Z. Wang, J. Zhao, J. Huang, L. Luo, D. Liu, S. Yang, H. Guo, and Z. Li, "Integrated chalcogenide photonics for microresonator soliton combs," Laser Photonics Rev. **17**, 2200219 (2022).
[35]M. Pu, L. Ottaviano, E. Semenova, and K. Yvind, "Efficient frequency comb generation in AlGaAs-on-insulator," Optica **3**, 823–826 (2016).
[36]G. Moille, L. Chang, W. Xie, A. Rao, X. Lu, M. Davanço, J. E. Bowers, and K. Srinivasan, "Dissipative Kerr solitons in a III–V microresonator," Laser Photonics Rev. **14**, 2000022 (2020).
[37]A. Nardi, A. Davydova, N. Kuznetsov, M. H. Anderson, C. Möhl, J. Riemensberger, P. Seidler, and T. J. Kippenberg, "Soliton microcomb generation in a III–V photonic crystal cavity," arXiv:2304.12968 (2023).
[38]B. Stern, X. Ji, Y. Okawachi, A. L. Gaeta, and M. Lipson, "Battery-operated integrated frequency comb generator," Nature **562**, 401–405 (2018).
[39]J. Liu, H. Tian, E. Lucas, A. S. Raja, G. Lihachev, R. N. Wang, J. He, T. Liu, M. H. Anderson, W. Weng, S. A. Bhave, and T. J. Kippenberg, "Monolithic piezoelectric control of soliton microcombs," Nature **583**, 385–390 (2020).
[40]A. S. Voloshin, N. M. Kondratiev, G. V. Lihachev, J. Liu, V. E. Lobanov, N. Y. Dmitriev, W. Weng, T. J. Kippenberg, and I. A. Bilenko, "Dynamics of soliton self-injection locking in optical microresonators," Nat. Commun. **12**, 235 (2021).
[41]C. Xiang, J. Liu, J. Guo, L. Chang, R. N. Wang, W. Weng, J. Peters, W. Xie, Z. Zhang, J. Riemensberger, J. Selvidge, T. J. Kippenberg, and J. E. Bowers, "Laser soliton microcombs heterogeneously integrated on silicon," Science **373**, 99–103 (2021).
[42]M. Churaev, R. N. Wang, A. Riedhauser, V. Snigirev, T. Blésin, C. Möhl, M. H. Anderson, A. Siddharth, Y. Popoff, U. Drechsler, D. Caimi, S. Hönl, J. Riemensberger, J. Liu, P. Seidler, and T. J. Kippenberg, "A heterogeneously integrated lithium niobate-on-silicon nitride photonic platform," Nat. Commun. **14**, 3499 (2023).
[43]Y. Liu, Z. Qiu, X. Ji, J. He, J. Riemensberger, A. S. Raja, W. Weng, J. Liu, and T. J. Kippenberg, "A photonic integrated circuit-based erbium-doped amplifier," Science **376**, 1309–1313 (2022).
[44]C. Op de Beeck, B. Haq, L. Elsinger, A. Gocalinska, E. Pelucchi, B. Corbett, G. Roelkens, and B. Kuyken, "Heterogeneous III–V on silicon nitride amplifiers and lasers via microtransfer printing," Optica **7**, 386–393 (2020).
[45]Q. Li, T. C. Briles, D. A. Westly, T. E. Drake, J. R. Stone, B. R. Ilic, S. A. Diddams, S. B. Papp, and K. Srinivasan, "Stably accessing octave-spanning microresonator frequency combs in the soliton regime," Optica **4**, 193–203 (2017).
[46]M. Gao, Q.-F. Yang, Q.-X. Ji, H. Wang, L. Wu, B. Shen, J. Liu, G. Huang, L. Chang, W. Xie, S.-P. Yu, S. B. Papp, J. E. Bowers, T. J. Kippenberg, and K. J. Vahala, "Probing material absorption and optical nonlinearity of integrated photonic materials," Nat. Commun. **13**, 3323 (2022).
[47]V. Brasch, M. Geiselmann, M. H. P. Pfeiffer, and T. J. Kippenberg, "Bringing short-lived dissipative Kerr soliton states in microresonators into a steady state," Opt. Express **24**, 29312–29320 (2016).
[48]X. Yi, Q.-F. Yang, K. Youl Yang, and K. Vahala, "Active capture and stabilization of temporal solitons in microresonators," Opt. Lett. **41**, 2037–2040 (2016).
[49]J. R. Stone, T. C. Briles, T. E. Drake, D. T. Spencer, D. R. Carlson, S. A. Diddams, and S. B. Papp, "Thermal and nonlinear dissipative-soliton dynamics in Kerr-microresonator frequency combs," Phys. Rev. Lett. **121**, 063902 (2018).
[50]H. Zhou, Y. Geng, W. Cui, S.-W. Huang, Q. Zhou, K. Qiu, and C. Wei Wong, "Soliton bursts and deterministic dissipative Kerr soliton generation in auxiliary-assisted microcavities," Light: Sci. Appl. **8**, 50 (2019).
[51]S. Zhang, J. M. Silver, L. Del Bino, F. Copie, M. T. M. Woodley, G. N. Ghalanos, A. Ø. Svela, N. Moroney, and P. Del'Haye, "Sub-milliwatt-level microresonator solitons with extended access range using an auxiliary laser," Optica **6**, 206–212 (2019).
[52]T. E. Drake, J. R. Stone, T. C. Briles, and S. B. Papp, "Thermal decoherence and laser cooling of Kerr microresonator solitons," Nat. Photonics **14**, 480–485 (2020).
[53]H. Zhang, L. Lu, J. Chen, and L. Zhou, "Program-controlled single soliton generation driven by the thermal-compensated avoided mode crossing," J. Lightwave Technol. **41**, 1801–1810 (2023).
[54]L. Zhou, Y. Shen, C. Xi, X. Huang, and G. He, "Computer-controlled microresonator soliton comb system automating soliton generation and expanding excursion bandwidth," Opt. Continuum **1**, 161–170 (2022).
[55]J. K. Jang, M. Erkintalo, S. Coen, and S. G. Murdoch, "Temporal tweezing of light through the trapping and manipulation of temporal cavity solitons," Nat. Commun. **6**, 7370 (2015).
[56]T. Wildi, V. Brasch, J. Liu, T. J. Kippenberg, and T. Herr, "Thermally stable access to microresonator solitons via slow pump modulation," Opt. Lett. **44**, 4447–4450 (2019).
[57]K. Nishimoto, K. Minoshima, T. Yasui, and N. Kuse, "Thermal control of a Kerr microresonator soliton comb via an optical sideband," Opt. Lett. **47**, 281–284 (2022).
[58]D. C. Cole, J. R. Stone, M. Erkintalo, K. Y. Yang, X. Yi, K. J. Vahala, and S. B. Papp, "Kerr-microresonator solitons from a chirped background," Optica **5**, 1304–1310 (2018).
[59]R. Miao, C. Zhang, X. Zheng, X. Cheng, K. Yin, and T. Jiang, "Repetition rate locked single-soliton microcomb generation via rapid frequency sweep and sideband thermal compensation," Photonics Res. **10**, 1859–1867 (2022).
[60]E. Obrzud, S. Lecomte, and T. Herr, "Temporal solitons in microresonators driven by optical pulses," Nat. Photonics **11**, 600–607 (2017).
[61]F. Lei, Z. Ye, and V. Torres-Company, "Thermal noise reduction in soliton microcombs via laser self-cooling," Opt. Lett. **47**, 513–516 (2022).
[62]D. Grassani, H. El Dirani, F. A. Sabattoli, L. Youssef, C. Petit-Etienne, S. Kerdiles, E. Pargon, M. Liscidini, C. Sciancalepore, D. Bajoni, and M. Galli, "Extending thermal stability of short-living soliton states in silicon nitride microring resonators," Opt. Continuum **1**, 1516–1528 (2022).

31 July 2024 01:40:19


© Author(s) 2023

[63]Z. Lu, H.-J. Chen, W. Wang, L. Yao, Y. Wang, Y. Yu, B. E. Little, S. T. Chu, Q. Gong, W. Zhao, X. Yi, Y.-F. Xiao, and W. Zhang, "Synthesized soliton crystals," Nat. Commun. **12**, 3179 (2021).
[64]V. Brasch, E. Lucas, J. D. Jost, M. Geiselmann, and T. J. Kippenberg, "Self-referenced photonic chip soliton Kerr frequency comb," Light: Sci. Appl. **6**, e16202 (2016).
[65]T. Carmon, L. Yang, and K. J. Vahala, "Dynamical thermal behavior and thermal self-stability of microcavities," Opt. Express **12**, 4742–4750 (2004).
[66]H. Guo, M. Karpov, E. Lucas, A. Kordts, M. H. P. Pfeiffer, V. Brasch, G. Lihachev, V. E. Lobanov, M. L. Gorodetsky, and T. J. Kippenberg, "Universal dynamics and deterministic switching of dissipative Kerr solitons in optical microresonators," Nat. Phys. **13**, 94–102 (2017).
[67]Z. Ye, H. Jia, Z. Huang, C. Shen, J. Long, B. Shi, Y.-H. Luo, L. Gao, W. Sun, H. Guo, J. He, and J. Liu, "Foundry manufacturing of tight-confinement, dispersion-engineered, ultralow-loss silicon nitride photonic integrated circuits," Photonics Res. **11**, 558–568 (2023).
[68]Y.-H. Luo, B. Shi, W. Sun, R. Chen, S. Huang, Z. Wang, J. Long, C. Shen, H. Jia, Z. Ye, H. Guo, and J. Liu, "A wideband, high-resolution vector spectrum analyzer for integrated photonics," arXiv:2304.04295 (2023).

31 July 2024 01:40:19


© Author(s) 2023